

HPD COURIER

NUMBER 5 | SEPTEMBER 2023

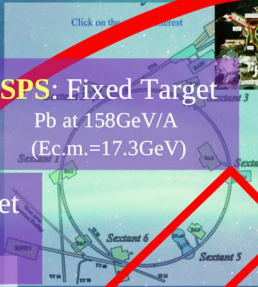
LHC: Collider
Pb+Pb @5020GeV/A



RHIC: Collider
Au+Au @ 200GeV/A



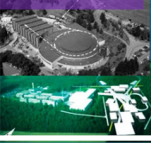
SPS: Fixed Target
Pb at 158GeV/A
(Ec.m.=17.3GeV)



AGS: Fixed Target
Au at 11.7GeV/A
(Ec.m.=4.86GeV)



Bevalac
Fixed Target
1-2GeV/A



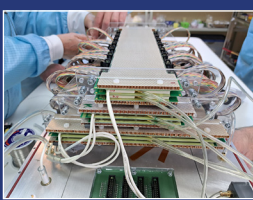
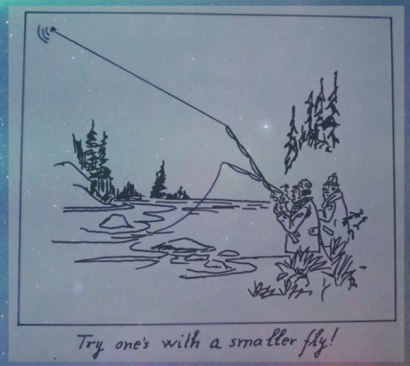
BES

SIS 18

- Hotter
- Faster
- Longer
- Bigger



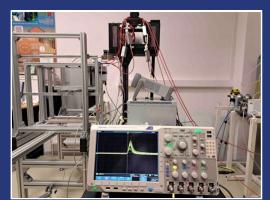
???



The three types of direct gas flow MSMGRPS



TRD-2D final design, assembled and tested



Contents

Achievements

- Nuclear Structure and Dynamics 2
 - 1. Shape coexistence and isomeric states in ^{94}Pd within a beyond-mean-field approach
 - 2. E0 transition strengths in ^{70}Se and ^{70}Kr mirror nuclei within a beyond-mean-field model
- Strongly Interacting Matter 4
 - 1. Features of hadronic and deconfined matter at collision energies available from the BNL Alternating Gradient Synchrotron to the CERN Large Hadron Collider
 - 2. Features of strangeness production in pp and heavy ion collisions
- R&D activities 11
 - 1. RPC @ mCBM
 - 2. TRD2D @ mCBM 2022
 - 3. Demonstrating the x-y position sensitivity capabilities of the TRD2D using the mCBM setup
 - 4. Using the TRD2D
for debugging and aligning the mCBM 2022 setup
 - 5. Using the TRD2D
for accessing the low- p_T proton component @ CBM
 - 6. Energy reconstruction with TRD2D
preparing the system for real life applications
- Applied Research 18
 - Deposition of TiO_2 + GO nanomaterials from colloidal dispersion in water on metallic substrates by electrophoretic method
- Infrastructure 19
 - Computing

Events

- The 42nd CBM Collaboration Meeting 20
- Summer Student Program 20
- Students' activity & teaching 21
- Visits 22
- Participation at international conferences 23
- Other events 26
- Job opportunities 27

Nuclear Structure and Dynamics

1. Shape coexistence and isomeric states in ^{94}Pd within a beyond-mean-field approach

The heaviest nuclei around the $N=Z$ line offer new insights into the coexistence phenomena and the fundamental symmetries. These exotic nuclei are of particular interest due to the open questions concerning the nature of the observed isomers, the irregularities in the excitation spectra and their feeding by the β decay of the neighboring nuclei. We investigated the evolution of shape coexistence and mixing in the structure of ^{94}Pd positive parity states and the nature of the isomeric states at spin 8^+ and 14^+ as well as the feeding of ^{94}Pd by the Gamow-Teller β decay of the 7^+ isomer and the superallowed Fermi β decay of the 0^+ ground state of ^{94}Ag .

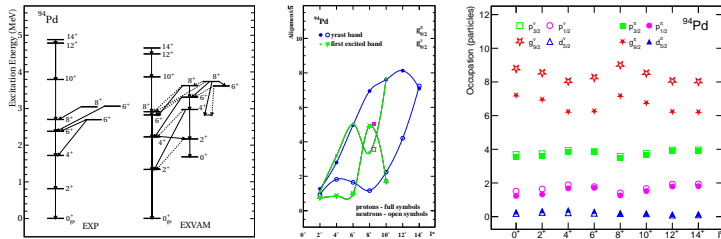


Figure 1: Left: Spectrum of positive parity states in ^{94}Pd ; Middle: Alignment plot in ^{94}Pd ; Right: Occupation of spherical orbitals in ^{94}Pd .

The beyond mean-field description of the effects of shape coexistence and mixing on the structure and dynamics of the investigated states in ^{94}Pd and ^{94}Ag is achieved within the *complex* Excited Vampir model using a realistic effective interaction derived from a nuclear matter G-matrix based on the Bonn CD potential. The competition between $T=0$ and $T=1$ neutron-proton and like-nucleon pairing correlations is self-consistently taken into account by the underlying essentially *complex* Hartree-Fock-Bogoliubov transformations.

The evolution of shape coexistence and mixing with increasing spin and excitation energy corroborated with the change in the alignment of the protons and neutrons occupying the $0g_{9/2}$ spherical orbital are responsible for the isomeric nature of the yrast 8^+ and 14^+ states. The observed decay pattern of the lowest 6^+ and 8^+

states in ^{94}Pd populated in the Gamow-Teller β -decay of the 7^+ isomer in ^{94}Ag is supported by the predicted changes in the shape mixing. The comparison with the available experimental data indicates rather good agreement and supports our scenario on the evolution of the shape coexistence and mixing in the ^{94}Pd nucleus.

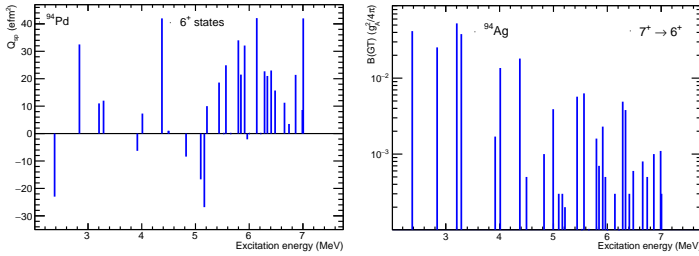


Figure 2: Left: Spectroscopic quadrupole moments of 6^+ states in ^{94}Pd ; Right: Gamow-Teller strength distribution for the decay of the 7^+ isomer in ^{94}Ag to 6^+ states in ^{94}Pd .

For details

A. S. Mare and A. Petrovici, *Phys. Rev. C* 106, 054306 (2022).

A. S. Mare, PhD thesis: *Nuclear Structure and Dynamics of Exotic Medium-Mass Nuclei*, Doctoral School in Physics, University of Bucharest, 2022 (Coordinator: A. Petrovici).

2. $E0$ transition strengths in ^{70}Se and ^{70}Kr mirror nuclei within a beyond-mean-field model

The characteristic properties of proton-rich nuclei in the $A=70$ mass region are essentially affected by the evolution of shape mixing with increasing excitation energy and spin and significantly influenced by the competing neutron-proton pairing correlations in both $T=0$ and $T=1$ channels and the like-nucleon ones as well as the isospin-symmetry violation interactions. The electric monopole transitions ($E0$) are a sensitive probe for the realistic understanding of the shape coexistence and mixing effects. The description of the coexisting configurations displaying different intrinsic deformations in the structure of the involved wave functions is a challenge and test of nuclear models. In the recent years $E0$ transitions have become a key observable in the experiments and the theoretical investigations. Presently, not only the $E0$ transitions between the 0^+ states, but also between the lowest 2^+ and 4^+ states are considered relevant fingerprints of shape coexistence and mixing.

The evolution of shape coexistence and mixing and the strengths of the $E0$ transitions in the mirror nuclei ^{70}Se and ^{70}Kr are investigated in the frame of the beyond-mean-field *complex* Excited Vampir variational model with variation after

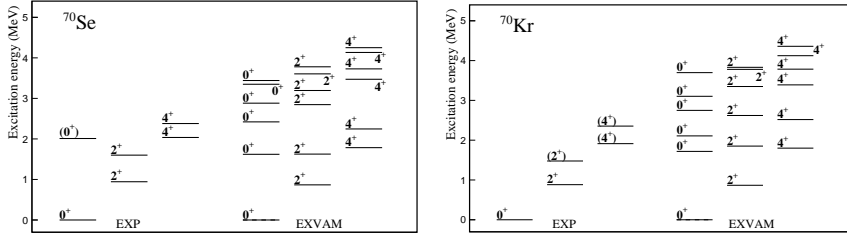


Figure 3: Spectrum of the lowest 0^+ , 2^+ , and 4^+ states in ^{70}Se (left) and ^{70}Kr (right).

symmetry projection. The effective interaction is obtained renormalizing a nuclear matter G-matrix based on the charge dependent Bonn CD potential in a rather large model space. The effects of shape mixing on the $E0$ transition strengths for the lowest few 0^+ , 2^+ , and 4^+ states as well as the $M1$ and $E2$ strengths for the $2_i^+ \rightarrow 2_j^+$ and $4_i^+ \rightarrow 4_j^+$ transitions were analyzed and discussed.

For details

A. Petrovici, *Symmetry* 14, 2594 (2022).

Strongly Interacting Matter

1. Features of hadronic and deconfined matter at collision energies available from the BNL Alternating Gradient Synchrotron to the CERN Large Hadron Collider

Previous extensive studies on the dependence of the average transverse momentum, its slope as a function of the hadron mass and the average transverse expansion on the particle multiplicity per unit rapidity and unit transverse overlap area of the colliding partners were extended to the ratio of the energy density to the entropy density. The dependence of the ratio of the energy density $\langle dE_T/dy \rangle / S_\perp$ to the entropy density $\langle dN/dy \rangle / S_\perp$ as a function on entropy density at different collision centralities for A-A collisions from the Alternating Gradient Synchrotron (AGS), Super Proton Synchrotron (SPS), Relativistic Heavy Ion Collider (RHIC) and Large Hadron Collider (LHC) energies is presented on the left side of Fig.1. On the right side of Fig.1 are shown the $\langle dE_T/dy \rangle / \langle dN/dy \rangle - \langle dN/dy \rangle / S_\perp$ correlations for the overlap transverse areas $S_\perp \approx 24, 64, 108$ and 149 fm^2 . The lines represent the result of fitting the corresponding points with a 4th degree polynomial. A clear dependence on the size of the transverse overlap area is observed.

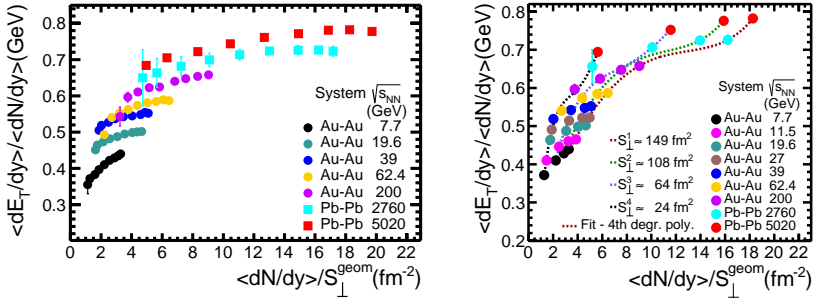


Figure 1: Left: the $\langle dE_T/dy \rangle / \langle dN/dy \rangle - \langle dN/dy \rangle / S_{\perp}$ correlation for different collision energies and different centralities. Right: the $\langle dE_T/dy \rangle / \langle dN/dy \rangle - \langle dN/dy \rangle / S_{\perp}$ for four values of the transverse overlapping area.

The rise in $\langle dE_T/dy \rangle / \langle dN/dy \rangle$ at RHIC energies becomes steeper and the range in $\langle dN/dy \rangle / S_{\perp}$, corresponding to a close to a plateau trend, decreases from central to peripheral collisions and is expected to converge towards the values corresponding to minimum bias pp collisions in the same energy range, once the contribution from nucleons suffering single collisions becomes predominant. The pressure term in the equation of state could also contribute to the observed trend. Therefore, theoretical models taking into account all possible contributions such to reproduce the experimental trend are mandatory.

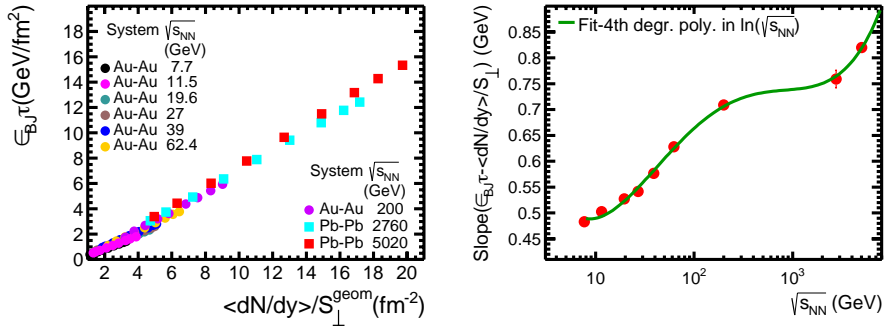


Figure 2: Left: The Bjorken energy density times the interaction time as a function of $\langle dN/dy \rangle / S_{\perp}$ for different A-A collision energies. Right: The slope of the $\epsilon_{Bj}\tau$ linear dependence on $\langle dN/dy \rangle / S_{\perp}$ as a function of the collision energy. The line is the result of the fit with a 4th order polynomial in $\ln(\sqrt{s_{NN}})$ and is used to guide the eye.

The dependence of the Bjorken energy density times the interaction time ($\epsilon_{Bj}\tau$) from AGS, SPS and RHIC energies on the particle multiplicity per unit rapidity and unit transverse overlap area $\langle dN/dy \rangle / S_{\perp}$ is presented in Fig.2-left. For each collision energy $\epsilon_{Bj}\tau$ shows a linear dependence on $\langle dN/dy \rangle / S_{\perp}$. The values of

the slope of this dependence, related to the temperature of the system, resulting from a linear fit of this correlation for each system and energy, as a function of collision energy are presented in Fig.2-right. The slope values increase from AGS to the highest RHIC energy. The values for LHC energies are larger and not in-line with what should be expected from a simple extrapolation of the trend observed at lower collision energies, thus suggesting a saturation or an inflection point within the energy gap between RHIC and LHC energies. The physics behind the increasing trend at LHC energies could be related to the large increase of the gluon density, therefore increasing the percolation probability, the ropes decay being at the origin of increased average transverse momentum.

In order to represent the same type of correlations for pp collisions at LHC energies an estimate of the transverse overlapping area is required. The transverse overlap area for pp collisions, $S_{\perp}^{pp} = \pi r_{max}^2$ as a function of charged particle multiplicity was estimated using the result of the IP-Glasma model, r_{max} being the maximal radius for which the energy density of the Yang-Mills fields is above $\varepsilon = \alpha \Lambda_{QCD}^4$ ($\alpha \in [1, 10]$, A. Bzdak et. al., Phys. Rev. C 87, 064906 (2013)). The model results for $\alpha = 1$ were fitted with:

$$f_{pp} = \begin{cases} 0.387 + 0.0335x + 0.274x^2 - 0.0542x^3 & \text{if } x < 3.4 \\ 1.538 & \text{if } x \geq 3.4 \end{cases} \quad (1.1)$$

Using the same recipe we fitted the r_{max} values for $\alpha=10$ with the following expression:

$$f_{pp} = \begin{cases} -0.18 + 0.3976x + 0.095x^2 - 0.028x^3 & \text{if } x < 3.4 \\ 1.17 & \text{if } x \geq 3.4 \end{cases} \quad (1.2)$$

where $x=(dN/dy)^{1/3}$ and $r_{max}=1\text{fm}\cdot f_{pp}(x)$. The transverse overlap area for pp MB collisions at lower energies was estimated using the Glauber MC approach at subnucleonic level.

The results are presented in Fig.3 in which, on top of the correlations evidenced in A-A collisions, by green line are represented the results for pp MB collisions and by up triangles ($\alpha=1$) and down triangles ($\alpha=10$) the results for pp collisions at LHC energies of 7 TeV and 13 TeV as a function of charged particle multiplicity. As could be seen in Fig.3 left, the trend observed in pp collisions for $\alpha=10$ is similar with the trend for Pb-Pb collision at 5.02 TeV. A bit larger values for pp at the same $\langle dN/dy \rangle / S_{\perp}$ could have the origin in the higher collision energies of pp collisions compared to those of Pb-Pb collisions. This is seen also in the difference between pp at 13 TeV relative to 7 TeV. As it was mentioned above, this is in line with the expectations based on the string percolation approach. The Bjorken energy density times the interaction time values for pp collisions at the two LHC energies as a function of $\langle dN/dy \rangle / S_{\perp}$ presented in Fig.3 right, using the same symbols as in Fig.3 left, are in very good agreement with the ones corresponding to Pb-Pb collision at $\sqrt{s_{NN}}=5.02$ TeV. For pp collisions the slopes of $\epsilon_{Bj}\tau$ as a function of $\langle dN/dy \rangle / S_{\perp}$ are 0.89 ± 0.09 GeV at $\sqrt{s} = 7$ TeV and 0.92 ± 0.07 GeV at $\sqrt{s} = 13$ TeV, respectively, for $\alpha = 10$, a bit larger values than that corresponding to the Pb-Pb collision at $\sqrt{s_{NN}} = 5.02$ TeV.

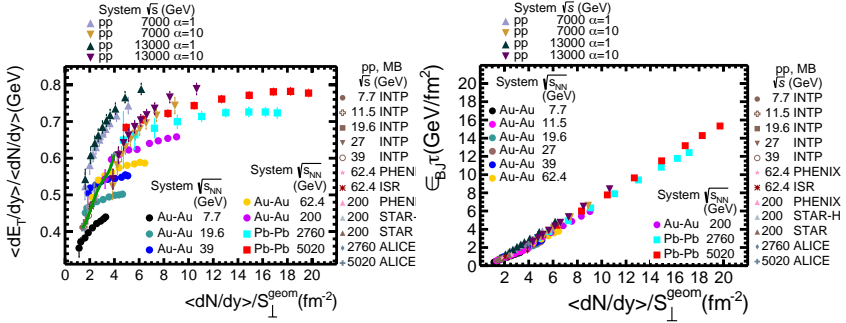


Figure 3: Left: The $\langle dE_T/dy \rangle / \langle dN/dy \rangle - \langle dN/dy \rangle / S_{\perp}$ correlation for A-A collisions, pp MB at the same energies (the green line) and pp as a function of charged particle multiplicity at $\sqrt{s} = 7$ and 13 TeV. Right: The same type of figure as left side, but for the Bjorken energy density times the interaction time as a function of $\langle dN/dy \rangle / S_{\perp}$.

These studies evidence a tendency towards saturation in the ratio of the energy density to the entropy density as a function of entropy density in qualitative agreement with theoretical predictions (J.-P. Blaizot and J.-Y. Ollitrault, Phys.Lett 191B(1987)21).

The Bjorken energy density times the interaction time has a linear dependence on the particle multiplicity per unit rapidity and unit transverse overlap area for a given collision energy.

The observed trend of the slopes of the $\epsilon_{Bj} \cdot \tau$ dependence on the entropy density $\langle dN/dy \rangle / S_{\perp}$, as a function of the collision energy, is similar with the ones evidenced in the $\langle dE_T/dy \rangle / \langle dN/dy \rangle - \langle dN/dy \rangle / S_{\perp}$ correlations.

The $\langle dE_T/dy \rangle / \langle dN/dy \rangle - \langle dN/dy \rangle / S_{\perp}$ and $\epsilon_{Bj} \cdot \tau - \langle dN/dy \rangle / S_{\perp}$ correlations for pp collisions at $\sqrt{s}=7$ TeV and 13 TeV follow qualitatively the ones corresponding to Pb-Pb collisions at $\sqrt{s_{NN}}=5.02$ TeV. Within the error bars, there is also a quantitative agreement if for S_{\perp} for the pp collision as a function of particle density only the region of overlap zone characterized by an energy density larger than ≈ 2 GeV/fm³ is considered. These are yet more similarities between Pb-Pb and pp collisions evidenced at LHC.

For details

M.Petrovici and A.Pop, Phys.Rev. C107(2023)034913.

M.Petrovici et al., "What is really new at LHC energies",

Carpathian Summer School of Physics, Sinaia, 2023:

[https://indico.nipne.ro/event/230/contributions/852/ attachments/429/734/mp_Sinaia_2023.pdf](https://indico.nipne.ro/event/230/contributions/852/attachments/429/734/mp_Sinaia_2023.pdf).

2. Features of strangeness production in pp and heavy ion collisions

40 years ago, long before the experimental data became available, the enhancement of the strangeness production was advocated as sensitive probe for deconfinement (J.Rafelski and B.Muller, Phys.Rev.Lett. 48(1982)1066). As far the centrality dependence of the strange hadron production is concerned, it was clearly shown that this is the result of the interplay between corona and core relative contribution, being a pure geometrical effect. Therefore, it cannot be considered as a signature of deconfinement. Once the experimental data at LHC energies on strangeness production were published, it has been shown that the ratio of strange hadrons yield relative to the entropy density for the most central collisions, qualitatively follows similar trend as the one observed in $\langle dE_T/d\eta \rangle / \langle dN_{ch}/d\eta \rangle - \langle dN/dy \rangle / S_\perp$ correlation (J. Rafelski and M. Petran, Acta Phys.Polon.Supp.7(2014) 35), indicative for a transition from hadronic gas to a mixed phase, hadronic and deconfined matter. Based on the most complete experimental information from AGS up to the LHC energies we performed a detailed study of the ratio of strange and multi-strange hadrons and anti-hadrons yield relative to the entropy density at different centralities and collision energies. Such a correlation for single strange anti-hadrons and four values of transverse overlapping area are presented in Fig.4.

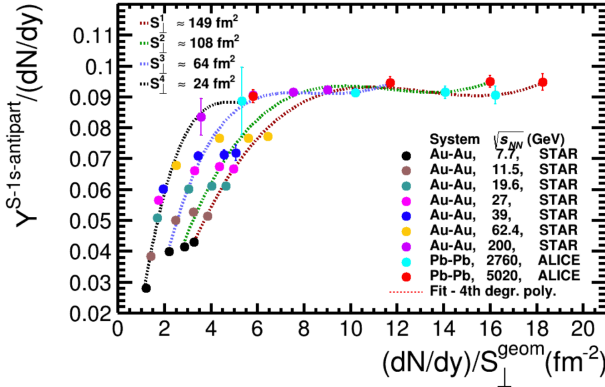


Figure 4: The ratio of the single-strange anti-hadrons density to the entropy density as a function of entropy density for four values of the transverse overlapping area.

As can be seen, a steeper increase of $Y^s/(dN/dy)$ as a function of entropy density is evidenced for lower values of transverse overlapping area, therefore, the plateau observed in such correlation is reached earlier. The values of $Y^s/(dN/dy)$ corresponding to the plateau does not show any dependence on the S_\perp . The range in the entropy density corresponding to the plateau increases with the fireball volume. At LHC energies, a slight increase of $Y^s/(dN/dy)$ at $\sqrt{s_{NN}}=5.02$ TeV relative to $\sqrt{s_{NN}}=2.76$ is observed.

The ratio between the multi-strange hadrons and anti-hadrons yield density per unit of rapidity and entropy as a function of entropy density is presented in Fig.5

left and Fig.5 right, respectively.

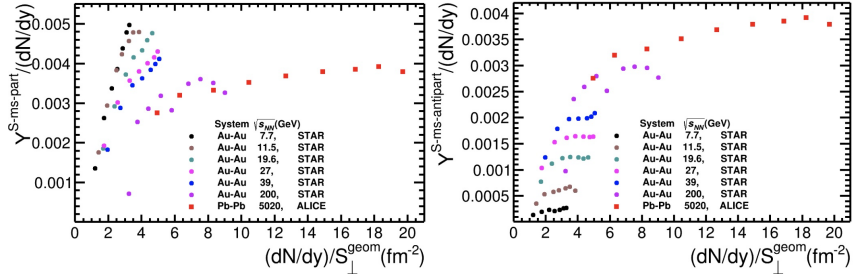


Figure 5: Left: the ratio of the multi-strange hadrons density to the entropy density as a function of entropy density; Right: the ratio of the multi-strange anti-hadrons' density to the entropy density as a function of entropy density from $\sqrt{s_{NN}}=7.7$ GeV up to 5.02 TeV.

The left plot of Fig.5 clearly shows that $Y^s/(dN/dy)$ for multi-strange hadrons increases with entropy density for a given collision energy and decreases with the collision energy as a consequence of their origin from binary collisions and the presence of baryonic matter in the region of mid-rapidity. The trend for the multi-strange anti-hadrons presented in Fig.5 right side is completely different, $Y^s/(dN/dy)$ increases with collision energy and for a given collision energy increases with entropy density, the bending towards larger entropy density, larger centrality, could be mainly due to the annihilation within the baryonic matter.

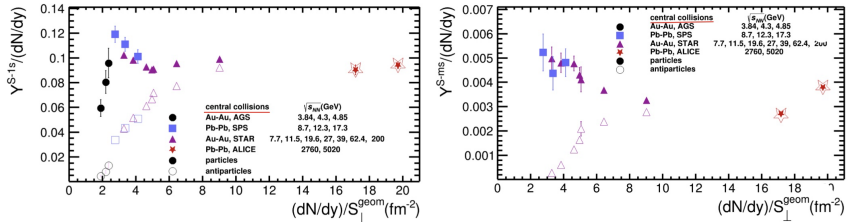


Figure 6: Left: $Y^s/(dN/dy) - (dN/dy)/S_{\perp}$ correlation for single strange hadrons (full symbols) and single-strange anti-hadrons (open symbols), from AGSI to LHC energies, for central collisions; Right: $Y^s/(dN/dy) - (dN/dy)/S_{\perp}$ for multi-strange hadrons (full symbols) and anti-hadrons (open symbols) for central collisions, from BES up to the LHC energies.

In Fig.6 are represented the $Y^s/(dN/dy) - (dN/dy)/S_{\perp}$ for single strange hadrons and single-strange anti-hadrons on the left side and for multi-strange hadrons and anti-hadrons on the right side, for central collisions. For single strange hadrons the data obtained at AGS energies are included. The observed kink in the correlation for single-strange hadrons around entropy density of $\sim 3 fm^{-2}$, would correspond to the maximum baryon density at mid-rapidity. Beyond this value, $Y^{1s}/(dN/dy)$ decreases and converges to the value of single-strange anti-hadrons at $\sqrt{s_{NN}}=200$ GeV. The $Y^{1s}/(dN/dy)$ for single strange anti-hadrons increases with $(dN/dy)/S_{\perp}$

up to the largest RHIC energies, the value corresponding to $\sqrt{s_{NN}}=200$ GeV being similar to the single-strange hadrons one. Unfortunately, there is no experimental information available yet between RHIC top energy and the lowest energy measured at LHC. As it is well known, at LHC energies, the yields of strange hadrons and anti-hadrons are the same, therefore the $Y^{1s}/(dN/dy)$ are the same at the corresponding entropies. Within the error bars, these values are the same as the one observed at $\sqrt{s_{NN}}=200$ GeV. As far as concerns the $Y^{ms}/(dN/dy) - (dN/dy)/S_{\perp}$ for multi-strange hadrons and anti-hadrons, presented in Fig.6 right, a similar decrease of $Y^{ms}/(dN/dy)$ for hadrons is observed from $\sqrt{s_{NN}}=7.7$ GeV to $\sqrt{s_{NN}}=200$ GeV. As far as the information below $\sqrt{s_{NN}}=7.7$ GeV energy does not exist, a similar kink as the one evidenced for single-strange hadrons can't be evidenced although, based on similar consideration, the same discontinuity is expected. It is also observed that from $\sqrt{s_{NN}}=2.76$ TeV to $\sqrt{s_{NN}}=5.02$ TeV the $Y^{ms}/(dN/dy)$ increases again relative to the constant value between $\sqrt{s_{NN}}=200$ GeV and 2.76 TeV.

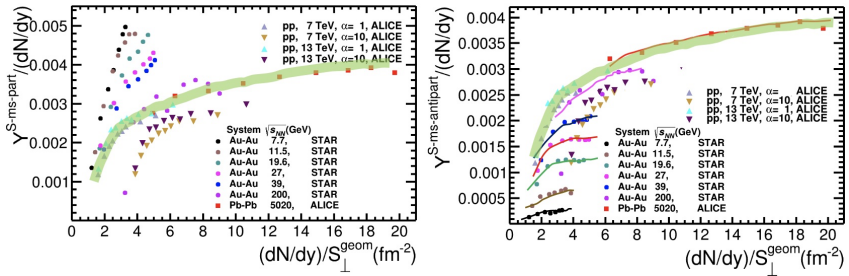


Figure 7: Left: the ratio of the multi-strange hadrons density to the entropy density as a function of entropy density; Right: the ratio of the multi-strange anti-hadrons' density to the entropy density as a function of entropy density. Up-triangles correspond to pp collisions for $\alpha=1$ and down-triangles to $\alpha=10$. Different colours are used for pp collisions at $\sqrt{s}=7$ and 13 TeV. The green bands are meant to guide the eye.

The comparison between the A-A and pp in terms of $Y^{ms}/(dN/dy) - (dN/dy)/S_{\perp}$ correlation for multi-strange hadrons and anti-hadrons is presented in Fig.7 left and right, respectively. For both, hadrons and anti-hadrons, the results for pp are on top of an extrapolation of Pb-Pb results towards lower entropy density. The green band is used only to guide the eye.

For details

M. Petrovici and A. Pop oral presentation at EuNPC 2022, October 24-28, 2022, University of Santiago de Compostela, Spain https://indico.cern.ch/event/1104299/contributions/5055299/attachments/2536779/4366087/EuNPC_talk_mp.pdf.

M.Petrovici et al., Carpathian Summer School of Physics, Sinaia, 2023:

https://indico.nipne.ro/event/230/contributions/852/attachments/429/734/mp_Sinaia_2023.pdf.

R&D activities

1. RPC @ mCBM

As it is well known, the long term operation of MRPCs with $C_2H_2F_4$ and SF_6 based gas mixtures leads to complex aging effects. In order to maintain the detector performance over the CBM lifetime, detailed aging investigation is of utmost importance. In the aging studies performed using a high activity ^{60}Co source existing in the Multipurpose Irradiation Facility (IRASM) of IFIN-HH, Bucharest, a gas pollution effect was evidenced by the depositions of chemical radicals on the anode side and by the ablation/etching processes on the cathode side of the resistive electrodes of a high counting rate MSMGRPC prototype. Enhanced depositions and higher noise rates were also observed around the spacers used for defining the gas gaps between the resistive electrodes. In the reported aging studies, the gas exchange inside the counter's gas gaps takes place via diffusion process. In order to avoid the deterioration of the counter's performance and to keep the electrode surface as clean as possible, MSMGRPC prototypes with a direct gas flow through the gaps between resistive electrodes were developed (Fig.1-left) and successfully tested in-beam in the mCBM experimental setup installed at SIS18/GSI Darmstadt.

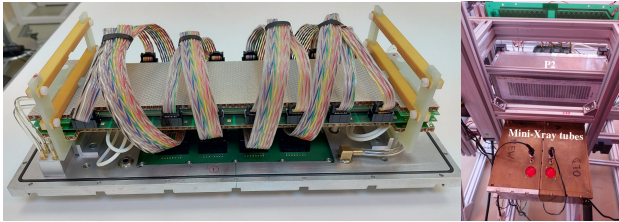


Figure 1: Left: the assembled direct flow prototype. Right: the experimental setup for the aging tests.

The first aging investigation for these prototype, was performed using the two Amptek mini-X ray tubes available in the detector laboratory of HPD/IFIN-HH. The tubes were aligned at about 14 cm in front of the chamber (Fig.1-right), exposing the full active area almost uniformly.

The influence of different gas flow rates on the decay of the dark current and dark counting rate after the end of each exposure was investigated. In Fig.2 one can observe the improvement brought by a higher gas flow rate on the dark current as well as on the dark counting rate of the chamber, confirming a gas pollution effect. For the results presented in Fig.2 a mixture containing 97.5% tetrafluoroethane and 2.5% SF_6 was used. Fig.3-left shows the influence on the dark current if a 5% iso- C_4H_{10} (isobutane) is added in the gas mixture. The dark current is the same for a gas flow rate of 4 l/h without isobutane as it is for a gas flow rate of 2 l/h with

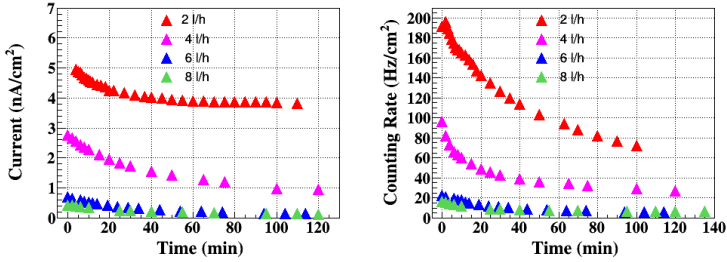


Figure 2: Dark current (left) and dark rate (right) vs. time, at different gas flow rates.

isobutane as it can be observed in Fig.3-right. Thus, to reduce the dark current and the dark counting rate for a certain gas flow rate it is necessary to include isobutane in the gas mixture.

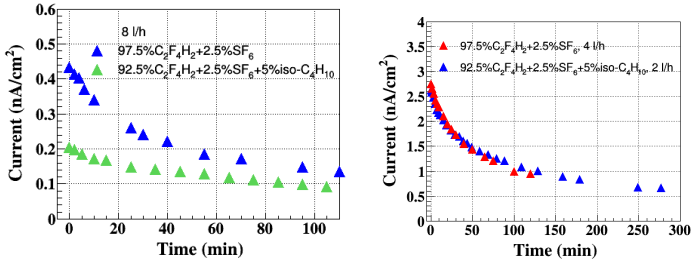


Figure 3: Left: dark current with and without isobutane for a gas flow of 8 l/h. Right: the same for 4 l/h without isobutane and 2 l/h with isobutane.

These results will be used for the optimization of the detector design, gas composition and gas flow rate in order to minimize the aging effects.

For details

D. Bartoř et al., Nuclear Inst. and Meth. in Phys. Res. A 1024 (2022) 166122.

M. Petriř et al., Nucl. Instrum. Meth. in Phys. Res. A 1045(2023) 167621.

M. Petriř et al., XVI Workshop on Resistive Plate Chambers and Related Detectors, September 26 - 30 2022, CERN, Geneva.

2. TRD2D @ mCBM 2022

The phase-0 of the CBM experiment, the mCBM setup, in Cave D of SIS18 facility of GSI/FAIR is foreseen to be a platform for test of detector prototypes and free-streaming readout electronics and data transfer to a computing farm as well as the online reconstruction and selection in a realistic environment which is expected to be 10 MHz interaction rate for CBM. Initiated in 2017, mCBM continued to take data during 2022. Preliminary tests of TRD2D detector continued in 2022 campaign with a FEE upgrade and inclusion in a wide range of data analysis with impressive results.

The number of read-out channels on the TRD2D module was increased from 144 to approx 1450. This upgrade included two more CROB boards and more LV units. The missing channels of this first generation FASPRO boards were masked Fig. 4 (3). Nevertheless the detector acceptance was good enough to cover the STS detector (bluish box in Fig. 4 (1)) and also most of the TRD1D (red in the same figure). The FEE was tested for a variety of particle multiplicities incident on the detector and no throttling was evidenced. We participated to every data taking run which was taken in the 2022 data-challenge campaign.

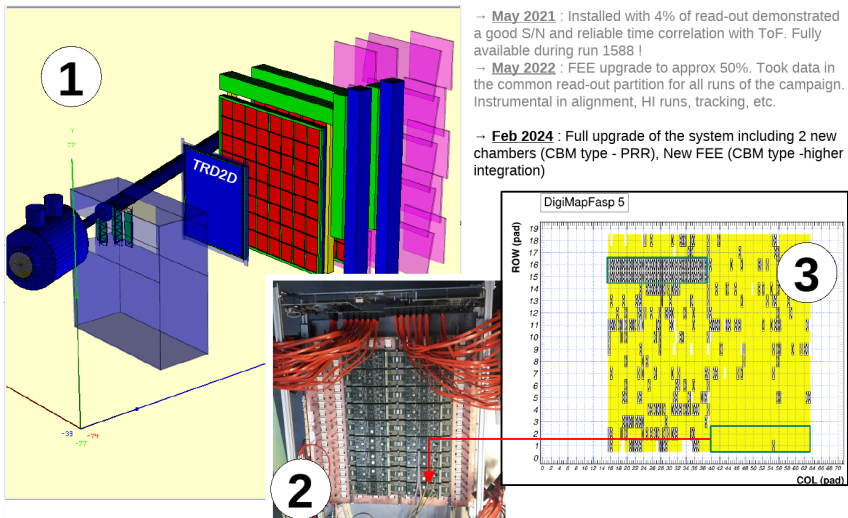


Figure 4: The TRD2D FEE upgrade of May 2022 in the context of previous and future developments. The position of the TRD2D in the mCBM setup (1), an image of the FEE on the back of the detector (2) and the map of active(yellow)/masked(crossed) channels on the detector.

For details

A. Bercuci et al., *CBM Operations Board*, <https://indico.gsi.de/event/17889/> (2023).

3. Demonstrating the x-y position sensitivity capabilities of the TRD2D using the mCBM setup

A first attempt to analyze the data was to build, on top of digi-events¹, spatial correlations between reconstructed hits in various systems (e.g. tracks). For this task, a simple seeding mechanism was proposed, by using the selection of digi-events with 2 STS hits in different units. Such seeds are linearly projected to the TRD2D detection plane and the matching with the closest TRD2D reconstructed hit is used to represent correlations.

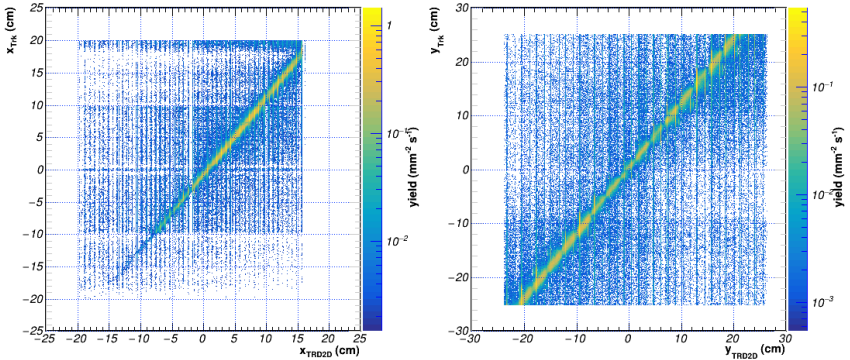


Figure 5: The spatial correlation in the horizontal - along anode wires (left) and vertical - across anode wires (right) of the reconstructed position of the TRD2D hits with tracks projected from the upstream STS detector.

In Fig. 5 the results of such a procedure are shown for both the horizontal (left panel) and vertical (right panel) directions. Of outermost importance, and to our knowledge a world premiere using such technologies, the vertical reconstruction improves the MWPC technology position resolution by more than an order of magnitude. The result was an unbiased and effective demonstration that we can cut costs and material budgets to 50 % wrt. the standard MWPC for position resolution estimates when using the 2D technology developed in the Hadron Physics Department (HPD).

For details

A. Bercuci et al., *CBM Technical Board*, <https://indico.gsi.de/event/15307/> (2022).

¹Digi-event definition and TRD2D data selection quality was already introduced in the previous number of HPD Courier.

4. Using the TRD2D for debugging and aligning the mCBM 2022 setup

The high position sensitivity of the TRD2D design was demonstrated for aligning the tracking detectors of the mCBM 2022 setup. An innovative method for aligning both the upstream STS and downstream ToF detectors was implemented using one TRD2D chamber and two standard TRDs for redundancy. The method is based on observing the deformations of an image when projected using misaligned reconstructed hits. The result of the method is to determine the real positions of the hits and thus straightening the projection.

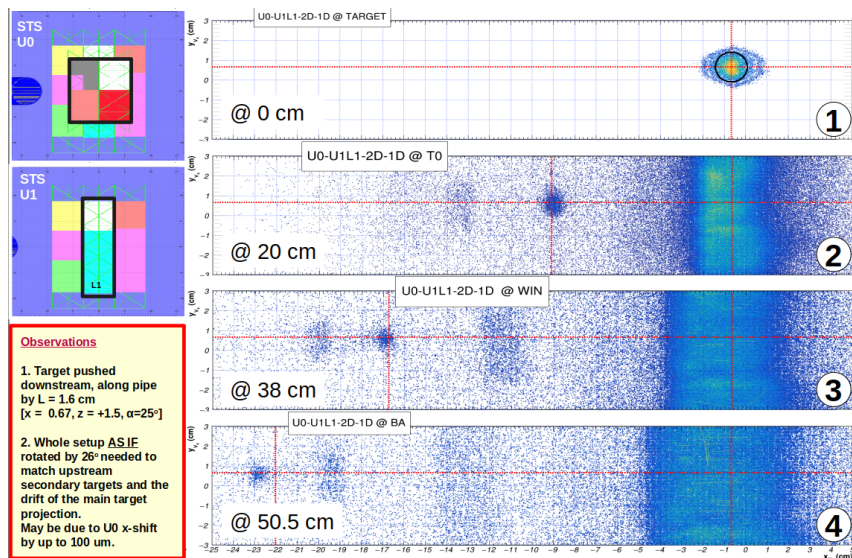


Figure 6: Reconstruction of main target (1) and various secondary targets from the target chamber of mCBM 2022 setup using the STS, TRD2D and TRD1D detectors.

After applying the alignment corrections, hits from STS and TRDs were used to make a tomography of the target chamber as shown in Fig. 6. Four focussing planes were selected at various upstream locations 0 (1), 20 (2), 38 (3) and 50.5 (4) cm) to search for main/secondary targets as defined by the mechanical design of the device. The intersection of dashed red lines points to the location of the target as derived from the CAD design while the focusing of tracks are experimental data. The matching between the CAD and reconstructed tracks is the proof of the correctness and precision of the alignment. Even a shift of the whole target chamber of 1.6 cm along the beam pipe was identified by a systematic study of the track focusing correlations (see "Observations" box in figure).

For details

A. Bercuci, 41st CBM Collab. Meeting, <https://indico.gsi.de/event/16428/contributions/70217> (2023).

C. Sturm et al., 41st CBM Collab. Meeting, <https://indico.gsi.de/event/16428/sessions/7939/> (2023).

5. Using the TRD2D

for accessing the low- p_T proton component @ CBM

Acceptance of the TRD2D design as part of the TRD system was conditioned by demonstrating the clear improvement of the new system and consequently the opening of new physics vistas. One such topic is the measurement of identified particle p_T spectra as low as possible to control integrated yield and to scan the phase space for theoretically predicted exotic phenomena. In Fig. 7 the mean p_T spectrum of the protons is shown as color code, over the area operated by the ten TRD2D in TRD station 1. The area emphasized by the red square is of particular interest as it coincides with the blind spot of the upstream STS tracker thus making the TRD2D the only tracker capable of identifying it and consequently accessing the $p_T < 200 \text{ MeV}/c$ region.

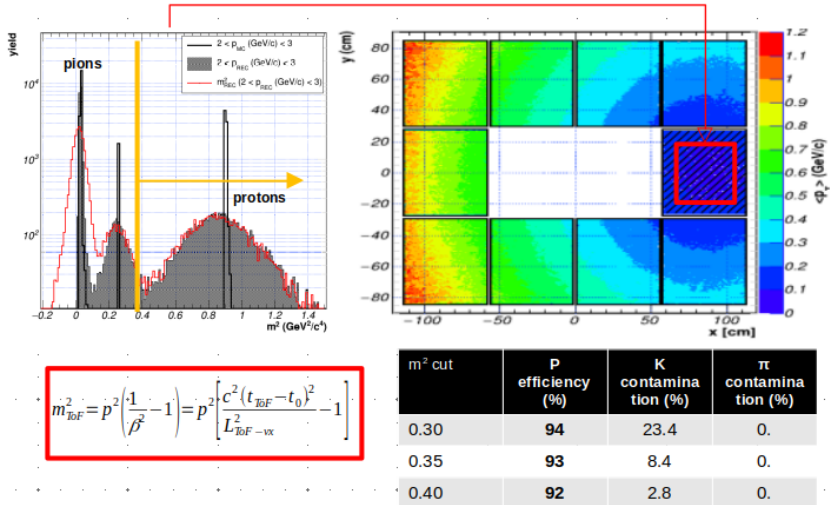


Figure 7: Realistic demonstration of the capabilities of the TRD2D system to expand the physics topics of CBM; the sensitivity of the system to low p_T protons (right) and the tracking/PID capabilities when correlated with ToF (left).

The physics case pointed out above was demonstrated for the FAIR referees based

on realistic simulations of the full CBM setup. A dedicated tracking code was developed for TRD2D which should work independent of STS. Also kinematics and particle identifications (PID) was demonstrated by matching with ToF. Finally a PID spectrum was reconstructed (Fig. 7 left / table) using only TRD2D tracks. For this result the TDR Addendum of the TRD2D was accepted and the TRD system was upgraded to a version having ten TRD2D modules in each of the 4 stations in the experimental demanding inner zone (small polar angles).

For details

A. Bercuci et al., *FAIR ECE/ECSS CBM break-out session*,
<https://indico.gsi.de/event/16075/> (2022).

6. Energy reconstruction with TRD2D preparing the system for real life applications

The participation in the mCBM 2022 setup was the occasion to test the full chain of data taking and detector modeling to its realistic limit. The apex of such chain is the determination of the energy loss by particle crossing the active area as it depends on a set of independent FEE channels of various build and working condition. An example of such variation is suggested in Fig. 8 (right) where the variation of the channel response (*Pad Id*) is registered for a fixed input delivered to the whole lot. Models describing the relevant chamber and ASIC behavior were developed to reproduce the measurements.

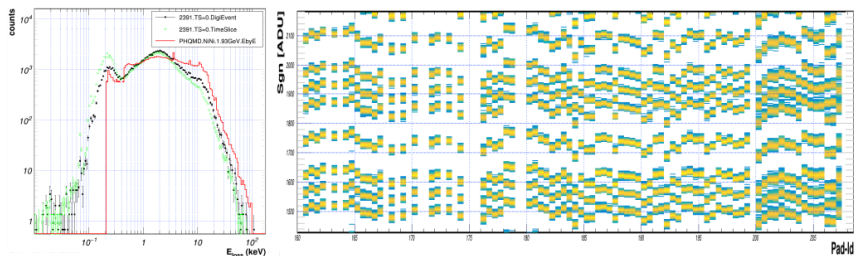


Figure 8: Energy loss reconstructed in TRD2D for three cases: PHQMD simulations [red line], measured Ni-Ni data with digi-event selection [black] and unbiased reconstructed hits from the same data set [green] (left); channel-to-channel variation in the FASP based FEE (right).

Fig. 8 (left) three energy loss spectra are compared for three cases of reconstruction setups. The red line represents simulations of central Ni-Ni collisions at 1.93 AGeV reconstructed using the ideal event-by-event (EbyE) scenario. The black markers represent the spectrum obtained from the reconstruction of a registered *timeslice*² of 10 ms length. The TRD2D reconstruction here is performed only for a selection

²CBM DAQ nomenclature for a self contained chunk of data.

determined by a trigger of T0, STS and ToF detectors (so-called Λ trigger) which cuts-out $\approx 75\%$ of registered data. Finally the green markers represent the energy reconstruction for the unbiased data taking of the same data chunk. The shape matching of the three spectra is the proof that the detector is realistically understood and well implemented in the CBM software and thus ready for physics. Quantitative variations between the spectra are due to calibration details - when data are compared to simulations - and to analysis bias when various reconstruction setups are compared.

For details

A. Bercuci, *mCBM Analysis Meeting*, <https://indico.gsi.de/event/17879/> (2023).

Applied Research

Deposition of $\text{TiO}_2 + \text{GO}$ nanomaterials from colloidal dispersion in water on metallic substrates by electrophoretic method

Electrophoretic method represents an extremely suitable coating method of nanomaterials on metallic substrates as, due to the electric field involved during the deposition process, it ensures a good adhesion to the metallic substrates.

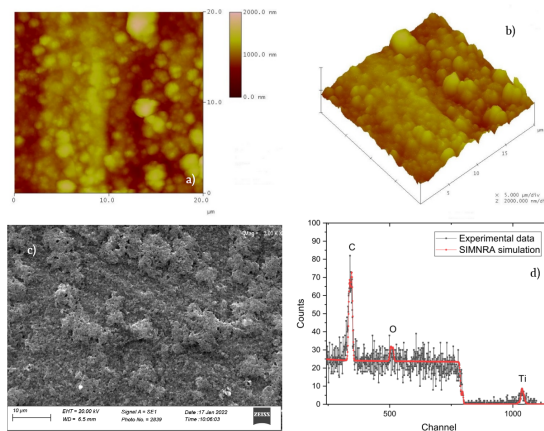


Figure 1: Characterization of the Aluminum surface deposited with $\text{TiO}_2 + \text{GO}$ (9:1) nanomaterials by electrophoretic method: a) 2D AFM image; b) 3D AFM image; c) SEM image; d) RBS spectrum.

We used a mixture of $\text{TiO}_2 + \text{GO}$ (9:1) nanomaterials in a colloidal dispersion of bi-distilled water and Chitosan (1%), having an electrophoretic cell of 70 ml full

capacity. The Aluminum substrate was treated before the deposition process in nitrogen vacuum plasma for surface activation, fast dried in UV irradiation after coating process and treated again in nitrogen vacuum plasma after its fast UV drying for a better adhesion to the metallic substrate. Adding chitosan to the water colloidal dispersion increased the mobility of the nanoparticles in the colloidal dispersions, while using both ultrasound bath before deposition process and ultra-sonication of the dispersion during the deposition process raised the degree of dispersed graphene, that meant a more uniform layer and finally, fast drying and nitrogen plasma treatment lead to a uniform and adherent TiO_2+GO coated film.

For details

RO-NO-0616 Project, TiO_2 nanotubes/graphene-based nanomaterials to address the emerging contaminants pollution, <https://www.itim-cj.ro/grafid/>

Infrastructure

Computing

The HPD Data Centre NIHAM is a Tier2 component of the ALICE GRID.



NIHAM maintains its efficiency within the ALICE GRID, last year $2.9 \cdot 10^6$ jobs being processed within 9.5 Mhours computing time, which amounts to 4% and 2.9% of Tier2 contributions to ALICE GRID, respectively. A new cooling unit was purchased and deployed this year. Also, 5 new computing servers (240 CPU cores) were purchased and successfully installed. In addition, the

deployment of the new servers and of the extension of the storage capacity are in progress. It is worth mentioning that the NAF computing center which is used for local needs is efficiently managed and running.

For details

<http://alimonitor.cern.ch/map.jsp>

Events

The 42nd CBM Collaboration Meeting

The 42nd CBM Collaboration Meeting will be organized by the Hadron Physics Department in the second half of September 2023.

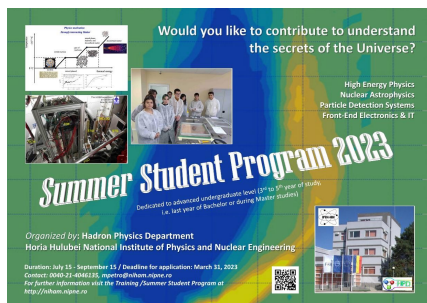
This will be a special meeting because we will celebrate the 20th anniversary of the CBM Collaboration. The event which will take place at HPD headquarters will also include a visit to Parliament House in Bucharest.

The CBM Juniors Day will take place one day before the Collaboration Meeting.



The poster for the 42nd CBM Collaboration Meeting features a central 3D cutaway diagram of the CBM experiment on the LHC horizon. Labels include PFD, CBM, TOF, TFD, MDC1, MDC2, MDC3, MDC4, MDC5, MDC6, MDC7, MDC8, MDC9, MDC10, MDC11, MDC12, MDC13, MDC14, MDC15, MDC16, MDC17, MDC18, MDC19, MDC20, MDC21, MDC22, MDC23, MDC24, MDC25, MDC26, MDC27, MDC28, MDC29, MDC30, MDC31, MDC32, MDC33, MDC34, MDC35, MDC36, MDC37, MDC38, MDC39, MDC40, MDC41, MDC42, MDC43, MDC44, MDC45, MDC46, MDC47, MDC48, MDC49, MDC50, MDC51, MDC52, MDC53, MDC54, MDC55, MDC56, MDC57, MDC58, MDC59, MDC60, MDC61, MDC62, MDC63, MDC64, MDC65, MDC66, MDC67, MDC68, MDC69, MDC70, MDC71, MDC72, MDC73, MDC74, MDC75, MDC76, MDC77, MDC78, MDC79, MDC80, MDC81, MDC82, MDC83, MDC84, MDC85, MDC86, MDC87, MDC88, MDC89, MDC90, MDC91, MDC92, MDC93, MDC94, MDC95, MDC96, MDC97, MDC98, MDC99, MDC100. The text on the poster reads: "42nd CBM Collaboration Meeting", "CBM Experiment on the horizon", "September 24-29, 2023 Bucharest, Romania", "Organized by Hadron Physics Department (HPD) Horia Hulubei National Institute for Physics and Nuclear Engineering", and "http://niham.nipne.ro e-mail: r.petro@nipne.ro". Logos for IFIN-HH, CBM, and various partners like INFN, FAIR, and others are at the bottom.

Summer Student Program



The poster for the Summer Student Program 2023 has a green and blue background. It features images of laboratory equipment and students working. The text includes: "Would you like to contribute to understand the secrets of the Universe?", "High Energy Physics Nuclear Astrophysics Particle Detection Systems Front-End Electronics & IT", "Summer Student Program 2023", "Dedicated to advanced undergraduate level (3rd to 5th year of study i.e. last year of bachelorette or during master studies)", "Organized by: Hadron Physics Department Horia Hulubei National Institute of Physics and Nuclear Engineering", "Deadline: July 15 - September 15 / Deadline for application: March 31, 2023", "Contact: 0040-21-4046123, niham@niham.nipne.ro", "For further information visit the Training/Summer Student Program at http://niham.nipne.ro", and a QR code.

This summer we are organizing another HPD Summer Student Program. The participants will be actively involved in the assembling of a new generation of MSMGRPC prototype based on discrete spacers. After a couple of introductory lectures on nuclear physics, they will be introduced to the most advanced topics covering detector physics and heavy ion physics.

For details

http://niham.nipne.ro/program_students.html

Students' activity & teaching

Theses

PhD thesis

A. S. Mare Nuclear structure and dynamics of exotic medium-mass nuclei

Master thesis

D. Dorobanțu An innovative architecture of Multi-Strip Multi-Gap Resistive Plate Counters for the inner zone of the Time-of-Flight system of the CBM experiment

A. G. Nan Visualisation of data and validation of reconstruction algorithms used in hadronic physics experiments

International events

Lectures

Prof. Dr. A. Petrovici Impact of shape coexistence on the dynamics of proton-rich and neutron-rich medium mass nuclei
Carpathian Summer School of Physics, July 2023,
Sinaia, Romania

Prof. Dr. M. Petrovici What is really new at LHC energies ?
Carpathian Summer School of Physics, July 2023,
Sinaia, Romania

National events

Talks

D. Dorobanțu An innovative architecture of Multi-Strip Multi-Gap Resistive Plate Counters for the inner zone of the Time-of-Flight system of the CBM experiment
Annual Scientific Session of Faculty of Physics, University of Bucharest, May 2023

Visits

The Hadron Physics Department hosted a series of visits during the last year. We are always honored and happy to present the infrastructure of our department, our research and results.



Among the most remarkable ones we could mention the visit of the CERN Council President, Prof. Dr. Eliezer Rabinovici.

Our department was also visited by the Romanian Minister of Research, Innovation and Digitalization, Sebastian I. Burduja.



We were glad to be visited by a group of students from Politehnica University of Bucharest. We introduced them to the fascinating world of physics.

Participation at international conferences

The members of our department have actively participated at various international conferences with invited talks and discussions about our physics proposals for the next generation of experiments.

We participated at Shapes and Symmetries in Nuclei: from Experiment to Theory, May 30 - June 3, 2022 at Orsay in France where we presented results on shape coexistence and β decay of neutron-rich medium mass nuclei.



ALICE Week June 6 - 10, 2022 at CERN. We were eager to see and discuss the latest results.



In October 24 - 28, 2022 we were at the European Nuclear Physics Conference (EuNPC) at Santiago de Compostela where we presented features of strangeness production in pp and heavy ion collisions.



The 40th CBM Collaboration Meeting took place in October 10 - 14, 2022 at Warsaw, Poland. Our latest developments on RPC and TRD detector prototypes were presented.



The 41st CBM Collaboration Meeting took place at Technische Universität, Darmstadt, Germany, March 6 - 10, 2023. We had a series of presentations showcasing our new architecture of the MSMGRPC detector. A quality test for the TRD chambers and an analysis of the alignment in the mCBM were also presented.



ALICE Physics Week took place in June 12 - 16, 2023 in Bucharest, Romania. We celebrated 30 years of ALICE Collaboration.



We participated at the CGS17 Conference organized in Grenoble, France, July 17 - 21, 2023 where we presented results on shape coexistence and mixing behind the isomers and β decay of heavy nuclei around the $N = Z$ line.

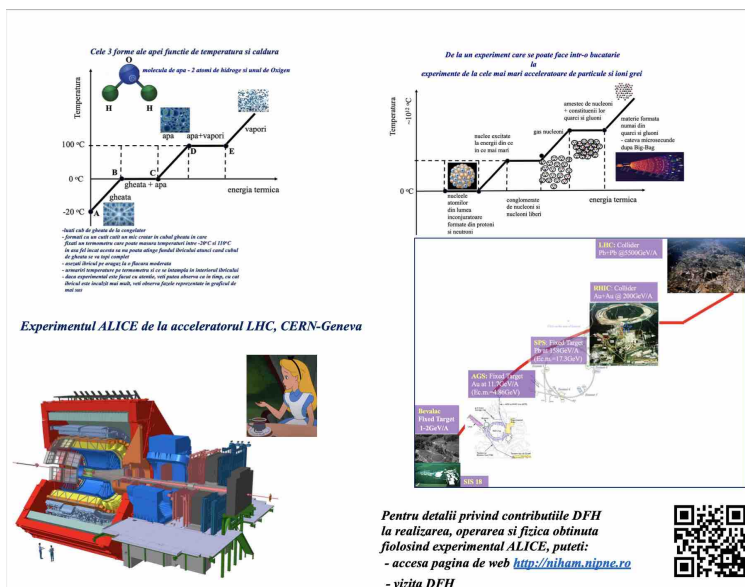


Other events

Dr. Iosif Charles Legrand has been awarded the title of Doctor Honoris Causa by the University Politehnica of Bucharest for "his exceptional contribution to science and technology, especially to the development of distributed systems." He is a Senior Researcher working at CERN for the ALICE collaboration involved in many activities taking place in our group over the years.



We participated with a poster at the Researchers Night about the signature of the phase transitions in nuclear matter.



Job opportunities

Physicist

Physicist from master student to postdoc level, to be involved in Experimental Heavy Ion Nuclear Physics and Theoretical Nuclear Astrophysics. The successful candidate will participate in research with members of the Hadron Physics Department from IFIN-HH, focusing on new generation of detectors construction, simulations, tests and their implementation in the CBM Experiment at FAIR. The candidate will also be involved in data analysis obtained in the test experiment at mCBM or in ALICE Experiment during Run3, starting from 2022.

Electronic Engineer

PhD or postdoc with some experience in CHIP design to be involved in development of analog and digital CHIPs for dedicated front-end electronics for the detectors developed in Hadron Physics Department for the present and future

experimental devices. The successful candidate will participate also in the test activities of the present CHIPs designed in HPD and produced, associated mother boards and should have knowledge on FPGA programming. The activities will be related to the CBM Experiment at FAIR and later to the future Heavy Ion Experiment at LHC.

Technician

Technician with a post high school certificate. The successful candidate will be involved in preparation of detector components, detector construction, operation and tests, maintenance and operation of the DetLabs infrastructure. Selected candidates will have a temporary position for 1 year with the possibility to be extended to 2 years. In case of high performance and adequate involvement in the HPD activities, the position could become permanent.

Contact

Prof. Dr. Mihai Petrovici
Email: mpetro@nipne.ro

Editors

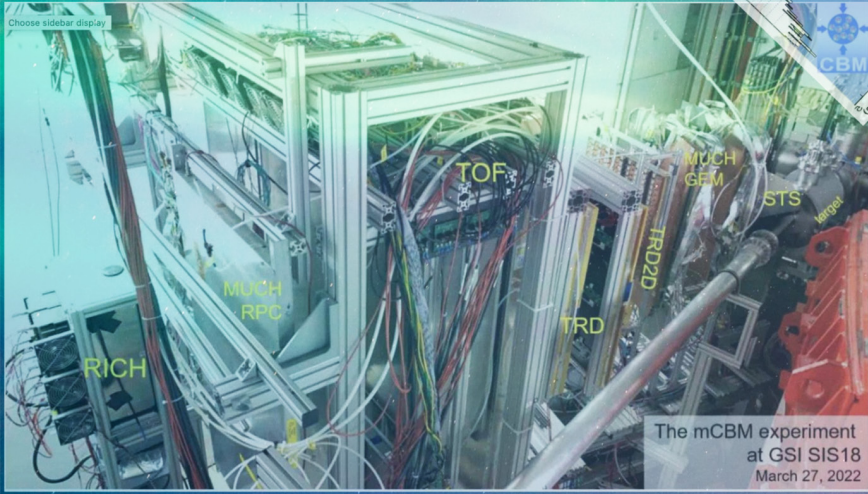
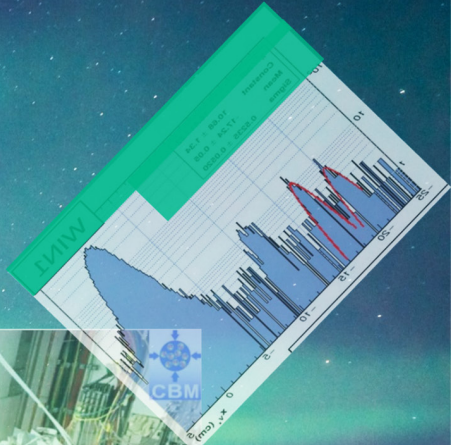
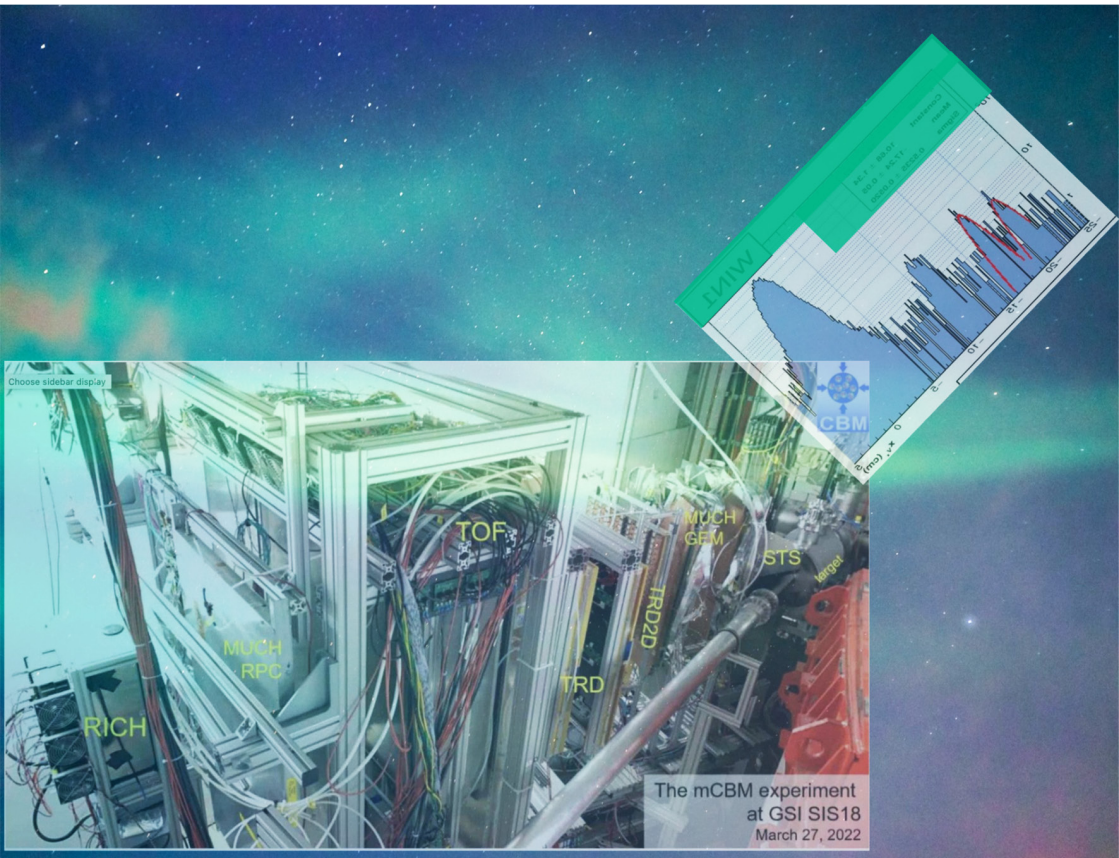
Mădălina Târzilă, Daniel Dorobanțu and Mihai Petrovici
Production editor: Adrian Socolov

Electronic version

HPD Couriers can be accessed at: http://niham.nipne.ro/HPD_Courier.html



Ministerul Cercetării,
Inovării și Digitalizării



The mCBM experiment
at GSI SIS18
March 27, 2022

*Email: mpetro@nipne.ro
Web: niham.nipne.ro*